Available online at www.sciencedirect.com
SCIENCE DIRECT®
Journal of Magnetic Resonance 169 (2004) 284–292
JMR Journal of Magnetic Resonance
www.elsevier.com/locate/jmr

Carr–Purcell echo spectra in the studies of lineshape effects. Nonclassical hindered rotation of methyl groups in 1,2,3,4-tetrachloro-9,10-dimethyltriptycene

P. Bernatowicz, I. Czerski, J. Jaźwiński, and S. Szymański*

Institute of Organic Chemistry, Polish Academy of Sciences, Kasprzaka 44/52, 01-224 Warszawa, Poland

Received 24 November 2003; revised 7 April 2004
Available online 7 June 2004

Abstract

In the standard NMR spectra, the lineshape patterns produced by a molecular rate process are often poorly structured. When alternative theoretical models of such a process are to be compared, even quantitative lineshape fits may then give inconclusive results. A detailed description is presented of an approach involving fits of the competing models to series of Carr–Purcell echo spectra. Its high discriminative power has already been exploited in a number of cases of practical significance. An explanation is given why it can be superior to methods based on the standard spectra. Its applicability in practice is now illustrated on example of the methyl proton spectra in 1,2,3,4-tetrachloro-9,10-dimethyltriptycene TCDMT. It is shown that, in the echo spectra, the recently discovered effect of nonclassical stochastic reorientation of the methyl group can be identified clearly while it is practically non-discernible in the standard spectra of TCDMT. This is the first detection of the effect at temperatures above 200 K. It is also shown that in computer-assisted interpretation of exchange-broadened echo spectra, the usual description of the stimulating radiofrequency pulses in terms of rotation operators ought to be replaced by a more realistic pulse model.

PACS: 82.56.Dj; 82.56.Jn; 33.25.+k; 33.15.Vb; 76.60 Es; 76.60 Lz

Keywords: NMR lineshape analysis; Carr–Purcell echo; Hindered rotation; Methyl group; Nonclassical stochastic dynamics

1. Introduction

The insight in molecular rate processes that can be gained from NMR lineshape studies is unique in its potential to discern even subtle details of the relevant microscopic mechanisms. Advances in the field by the end of the last decade were reviewed by Orrell [1]. In our recent research on hindered rotation of the methyl group, we were faced with a problem of discrimination between two models of the motion: the standard model of random, classical jumps between the equilibrium orientations, and the damped quantum rotor (DQR) model [2]. An essential difference between them is that in the former the NMR signal ought to be dependent on a single rate constant only, in agreement with the familiar Alexander–Binsch (AB) lineshape theory [3,4], while in the latter the signal shape is controlled by two rate processes. These are damping processes of certain specific quantum coherences between the torsional sublevels of the methyl rotor, which involve the spin and space nuclear coordinates entangled by the Pauli principle. The relevant coherences were once dubbed the overall tunneling and overall Kramers coherences [2]. When the two corresponding quantum rate constants, k_t and k_K, become equal, the DQR lineshape equation becomes equivalent to the AB equation. However, even in the latter instance the stochastic exchange becomes "classical" only in an operational sense, since the two coherence-damping processes described by k_K and k_t never merge into a single process. From extensive numerical simulations we could infer that, for the "nonclassicality coefficient" $c = k_t/k_K$ departing

* Corresponding author. Fax: +48-22-6326681.
E-mail address: sszym@icho.edu.pl (S. Szymański).

1090-7807/$ - see front matter © 2004 Elsevier Inc. All rights reserved.
doi:10.1016/j.jmr.2004.04.020

from 1 by less than 10%, there would be little chance to discriminate between the AB and DQR models solely on basis of the standard NMR spectra. More promising conclusions were drawn from simulations of various "echo" experiments, including the Carr–Purcell echo technique [5,6], in which a controlled delay between the end of the pulse sequence and start of acquisition of the FID signal is employed. These inferences helped us to confirm the validity of the DQR model in a broad range of temperatures. In the cryogenic region, the quantum character of the stochastic dynamics was identified for a CD_3 group in a molecular crystal [7]. Surprisingly, a similar behavior could be observed even above 170 K, in liquid-phase spectra of strongly hindered CH_3 groups in two 9-methyltriptycene derivatives, 1,2,3,4-tetrabromo-9-methyltriptycene TBMT, and 1,2,3,4-tetrachloro-9-methyltriptycene TCMT (see Fig. 1) [8,9]. In these systems, the nonclassicality coefficient c is different from 1 by about 20%. Unlike for the solid-state, in liquid-phase NMR a perfect theoretical reproducibility of the experimental lineshapes is in general achievable. Therefore, small but clearly visible deficiencies of the AB fits to the standard experimental spectra of the 9-methyltriptycenes, confronted with virtual perfection of the corresponding fits to the DQR model, are by themselves a sufficient proof of the validity of the latter. The CP-echo spectra were used essentially for a better visualization of the effect. For 1,2,3,4-tetrachloro-9,10-dimethyltriptycene TCDMT, the system studied presently, the situation is more difficult. For this compound, arguments based solely on the standard spectra are not convincing and use of the Carr–Purcell echo spectra is essential for the discrimination between the AB and DQR models. The conclusions are strengthened when the present results are compared with those previously obtained for the other 9-methyltriptycene derivatives. The challenging problem considered in this paper provides motivation to a detailed description of the experimental and numerical procedures that can be employed if faint lineshape effects are to be correctly interpreted. Although the present contribution is focused on exchange processes, most of the following argument will also be valid for nontrivial relaxation effects in NMR lineshapes.

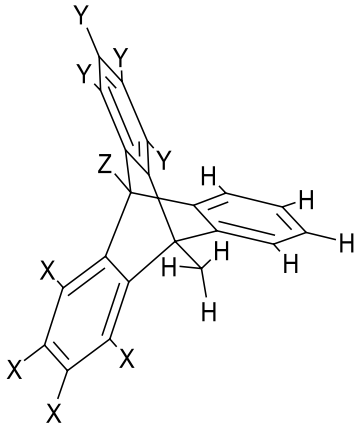

Fig. 1. The methyltriptycene derivatives investigated.

2. Experimental details

1,2,3,4-Tetrabromo-9,10-dimethyltriptycene TCDMT was synthesized from commercial (Aldrich) 9,10-dimethylanthracene and 1,2,3,4-tetrabromoanthranilic acid (obtained from commercial (Aldrich) 1,2,3,4-tetrabromophthalic anhydride), following strictly the published procedure for 1,2,3,4-tetrabromo-9-methyltriptycene [10]. Its structure was confirmed by NMR spectrum at room temperature: 7.508 ppm (m, 4), 7.183 ppm (m, 4), 2.880 ppm (s, 6); solvent: CS_2/CD_2Cl_2 (6 v/1 v). Variable temperature NMR measurements were performed on a Bruker Avance DRX 500 MHz spectrometer, equipped with a TBI probe and a BVT 3000 temperature unit, for a degassed solution of 3 mg TCDMT in 0.7 ml CS_2/CD_2Cl_2 (6 v/1 v) sealed under vacuum of about 0.1 Torr in an NMR tube (o.d. 5 mm). Temperature stability was ca. 0.1 K; the temperature was measured using the methanol chemical shift thermometer [11]. The methanol spectra were taken at every second temperature setting. At the intermediate temperatures, the temperature was calculated from thermocouple reads calibrated against the methanol chemical shift data for the neighboring temperature settings. The spectra of TCDMT were measured using calibrated π- and $\pi/2$-pulses of durations about 8 and 16 μs, respectively. In the standard experiments, the instrumental delay between the end of the pulse and start of the acquisition, Δ, was set at 6 μs. In all experiments, the repetition time was 6 s and the FID signal was collected (32 K data points) during a half of that time; the spectral width was ca. 5500 Hz. Usually, only 16 K (acquired during ca. 1.5 s) of the FID were used for FT-processing. In the frequency-domain spectra, no frequency-dependent phasing was used; the frequency-independent phase factor was adjusted manually to obtain a fair phasing in the methyl proton region. The methyl proton spectra subject to numerical analysis were described by 2200–3200 data points, depending on the extent of broadening. In the fits to sets of CP-echo spectra, each experimental spectrum in the input set was normalized in such a way that its maximum amplitude be 1. No statistical weighting of the data points from the individual spectra was employed.

3. Theory and computational procedures

The lineshape $Y(\omega)$ of a 1D NMR spectrum is described by the equation [3,4,12]:

$$Y(\omega) \propto \langle F_+|[-\mathrm{i}(\mathbf{L}+\omega\mathbf{1})+\mathbf{R}+\mathbf{X}]^{-1}|\rho_\mathrm{s}\rangle, \tag{1}$$

where **L**, **R**, and **X** are the superhamiltonian, the relaxation matrix, and the exchange superoperator, respectively; the supervectors $\langle F_+|$ and $|\rho_\mathrm{s}\rangle$ represent the total "spin-raising" operator $\hat{F}_+ = \hat{F}_x + \mathrm{i}\hat{F}_y$ and the relevant, single-quantum part of the spin density matrix at the start of acquisition of the FID signal, respectively. In the sequel, it is assumed that relaxation effects can be described by a single Lorentzian broadening w, the same for all resonances.

In an "ideal" standard 1D experiment, i.e., one performed using radiofrequency pulses of "infinitely short" duration, the relevant part of $\hat{\rho}_\mathrm{s}$ can be taken proportional to the spin-raising operator $\hat{F}_+$. In an "ideal" CP-echo experiment, set at the echo time τ, where both the initial $\pi/2$ and the refocusing π pulses are applied in direction x of the frame rotating with the pulse frequency ω_0, the initial density matrix entering Eq. (1) is given by

$$\begin{aligned}|\rho_\mathrm{s}(2\tau)\rangle \propto \exp\{[-\mathrm{i}(\mathbf{L}+\omega_0\mathbf{F}_z) - 2\pi w\mathbf{1} + \mathbf{X}]\tau\}\mathbf{P}_x(\pi)\\ \times \exp\{[-\mathrm{i}(\mathbf{L}+\omega_0\mathbf{F}_z) - 2\pi w\mathbf{1}\\ + \mathbf{X}]\tau\}\mathbf{P}_x(\pi/2)|F_z\rangle.\end{aligned} \tag{2}$$

In Eq. (2), $\mathbf{F}_z = \hat{F}_z \times \hat{I}^* - \hat{I} \times \hat{F}_z^*$ and $\mathbf{P}_x(\alpha)$ describes rotation by angle α about axis x of the rotating frame. Now, in the standard experiment, the exchange processes represented by **X** will be reflected in the lineshape only to the extent to which they can affect the course of the FID signal during the acquisition; the initial density matrix is independent of the system's internal dynamics. On the other hand, in the CP-echo experiments (and in echo experiments in general), the dynamics described by **X** can feature not only the course of the FID but the density matrix $\hat{\rho}_\mathrm{s}(2\tau)$ at the start of the FID acquisition as well. This is the reason why the CP-echo spectra can exhibit an enhanced sensitivity to details of the exchange mechanisms described by **X**. This remark is particularly true for series of echo spectra measured for appropriately chosen echo times. An enhanced sensitivity to details of exchange mechanism, observed for simulated multiple quantum spectra [13], can be rationalized in a similar way. As compared to the MQ spectra, experiments involving echo spectra are less time-consuming. The applicability of the echo techniques may by limited by the fact that all narrow impurity signals will be relatively amplified at longer echo times, causing distortions in the frequency range of interest. Also, when the signals of interest undergo "smearing" over a broad frequency range, the echo spectra will be of limited or no utility because of instrumental deformations in the detection of rapidly decaying signals.

In this paper, the discussion is focused on nonclassical stochastic behavior of strongly hindered methyl groups. The pertinent DQR exchange superoperator can be written as [2]:

$$\begin{aligned}\mathbf{X} = -\frac{k_\mathrm{K}}{3}[2\hat{I} \times \hat{I}^* - \hat{P} \times \hat{P}^* - \hat{P}^{-1} \times \hat{P}^{-1*}\\ + \frac{3(c-1)}{2}(\hat{I} \times \hat{I}^* - \hat{U} \times \hat{U}^*)],\end{aligned} \tag{3}$$

where $\hat{P}$ is the operator of cyclic permutation of the methyl proton spins, and $\hat{U} = \frac{1}{3}[2(\hat{P} + \hat{P}^{-1}) - \hat{I}]$ is a unitary selfinverse operator. When the nonclassicality coefficient $c = k_\mathrm{t}/k_\mathrm{K}$ equals 1, the AB superoperator describing the classical jump process of rate constant $k = k_\mathrm{K}/3 = k_\mathrm{t}/3$ is obtained, where k is an inverse of the mean residence time in one orientation. However, one has to remember that also in the latter instance the underlying stochastic process retains its composite character. It must also be stressed that for $c \neq 1$ it would be inappropriate to interpret the superoperator in the l.h.s. of Eq. (3) as one describing the classical hopping with rate constant $k = k_\mathrm{K}/3$ plus some sort of "incoherent tunneling" with rate constant $k' = k_\mathrm{K}(c-1)/2$. At cryogenic temperatures the values of c can drop below 1 [7] so that in such instances the alleged "incoherent tunneling" would have to occur with a negative rate constant! We have recently reported an alternative formulation of the exchange superoperator describing the effect concerned, which appears to be less prone to such a misinterpretation [14].

In our previous studies on the triptycene derivatives [8,9], we could identify this novel effect by a careful comparison of the fits of the AB and DQR lineshape equations to the experimental spectra. The FORTRAN routines once developed by us for the purposes of lineshape analysis in single-crystal spectra [7] were modified appropriately to handle liquid-phase spectra as well.

In all of the methyltriptycene derivatives investigated by us, including TCDMT, the methyl protons form an A_2B spin system showing no detectable J-couplings to other protons in the molecule. The choice of molecules with such a symmetry was motivated by the necessity of reducing to a minimum the number of spectral parameters to be adjusted in the iterative fits. On the other hand, the set of adjustable parameters must not be too small since discrepancies between the theoretical models and the spectra actually observed might also result from an inconsiderate fixing of some sensitive parameters of the theoretical lineshapes. The J-coupling constant between protons A and B, J, is an example of such a parameter. Unlike typical J-couplings between geminal protons attached to an aliphatic carbon atom, in both TCMT and TBMT the parameter J shows a significant dependence on temperature [9]. For this reason, the spectra of TCMT and TBMT could be interpreted quantitatively in relatively narrow temperature range in

which the parameter J could still be extracted from the spectra. Another important parameter is the "natural" linewidth w. For an A_2B spin system, the magnitude of w can be extracted from the spectrum as long as the resonances of protons A and B remain well-separated; this is because the exchange broadenings suffered by these resonances are not identical and are strictly interrelated. By and large, from our own experience with the methyltriptycene derivatives it follows that, in the slow exchange limit, the following spectral parameters can be simultaneously adjusted: k_K, c, J, w, the chemical shifts δ_A and δ_B, the overall amplitude factor, the slope and intercept of the baseline, and a parameter measuring admixture of dispersion in the nominally absorption spectrum. When some impurity signals of well-defined Lorentzian shape occur in the spectral region, they can also be included in the fits; three parameters are to be adjusted for each such signal: the width, position, and amplitude. When sets of CP-echo spectra are fitted, the "global" parameters k_K, c, J, w, δ_A, and δ_A are common for the entire set (as well as the widths and positions of the impurity signals). The remaining, "local" parameters involve the individual spectra. Of course, in the minimization routine employed by us (the Gauss–Newton algorithm) both the global and local parameters are treated on equal footing as they involve the same sum-of-squares surface.

For sets of (at least two) CP-echo spectra, it has proven advantageous (or, sometimes, even necessary) to abandon the standard assumption of ideal pulses that are represented by rotation superoperators. We generally use a more realistic description. The pulse of duration t_p, applied along axis x of the rotating frame, is described by the evolution superoperator representing a pulse with an ideal rectangular envelope,

$$|\rho(t+t_p)\rangle = \exp\{[-i(\mathbf{L}+\omega_0\mathbf{F}_z+\omega_1\mathbf{F}_x) - 2\pi w\mathbf{1} + \mathbf{X}]t_p\}|\rho(t)\rangle, \quad (4)$$

where for the nominal $\pi/2$- and π-pulses t_p is set equal to one-fourth and one-half, respectively, of the length of the 2π-pulse, determined by suitable calibration. The pulse strength, ω_1, is one more "global" parameter which is iteratively adjusted in the fitting procedure. The parameter ω_1 proves to be extractable from the sets of echo spectra in the slow exchange limit only, where the exchange term $\mathbf{X}$ is small in comparison with the imaginary terms. Thus, in practice this term (as well as the linewidth term) can be dropped from the exponent in Eq. (4) and the relevant calculations can be performed in Hilbert space,

$$\hat{\rho}(t+t_p) = \exp[-i(\hat{H}+\omega_0\hat{F}_z+\omega_1\hat{F}_x)t_p]\hat{\rho}(t)\exp[i(\hat{H} + \omega_0\hat{F}_z+\omega_1\hat{F}_x)t_p], \quad (5)$$

where $\hat{H}$ is the standard NMR Hamiltonian. In our calculations for three-proton systems, we used Eq. (4) despite of the fact that the usual factoring of the Liouville superoperators entering the exponent could not be benefited from (in presence of the radiofrequency term, invariance under rotations around z axis no longer exists). For such systems, the size of the complex matrix to be diagonalized is 64×64, and it drops to 40×40 when the selection rules generated by the existing C_s symmetry of the spin system are exploited. Numerical diagonalization of complex matrices of that size poses no problems in the fitting process. An implementation of the simplified expression in Eq. (5) would involve alterations of the logistic of our computer program which was originally designed to handle single-crystal spectra. When large spectral matrices are to be handled, the techniques exploiting the intrinsic sparsity of the Liouville superoperators may prove useful [18]. Some questions concerned with fitting of the effective pulse strength will be discussed further in the next section.

4. Results and discussion

In TCDMT, the two methyl groups are equivalent by symmetry (see Fig. 1). Because they occupy distant positions in the molecule, they can be treated as two independent DQR's. The standard spectra of the methyl protons in TCDMT were measured in the range 195 K—room temperature. At temperatures below 198 K and above 270 K the line broadenings due to the rate processes become comparable with the "natural" broadenings. In such instances, our assumption that the natural linewidth is the same for all resonances of the methyl protons may be insufficiently exact. Such spectra are not taken into account in the present studies. In the regime of slow exchange (198–210 K), which is of central interest here, apart from the standard spectra, two CP-echo spectra for suitably chosen echo times were measured at each temperature. Because of increased intensities of some impurity signals, echo spectra for longer echo times would be of a limited utility for quantitative fits. (The impurities, present in minute amounts, could not be removed completely using standard purification procedures; presumably, they originate in part from a spontaneous decomposition of the solvents used.) The fits of the AB and DQR equations to the standard spectra measured in the slow exchange limit are shown in Fig. 2. At a first glance, both of the models afford a fair reproduction of the experimental lineshapes. For the DQR fits, the RMS errors are consistently smaller, although the differences between the fits can hardly be visualized (unless one looks at the signals of proton B through a magnifying glass, see inset in Fig. 2). However, the nonclassicality coefficient c (set equal to 1 at the AB-stage of the iterative fit, and subject to adjustment at the DQR-stage) proves to be a sensitive parameter of the lineshape function. Its values, delivered by the fitting routine at convergence, are consistently

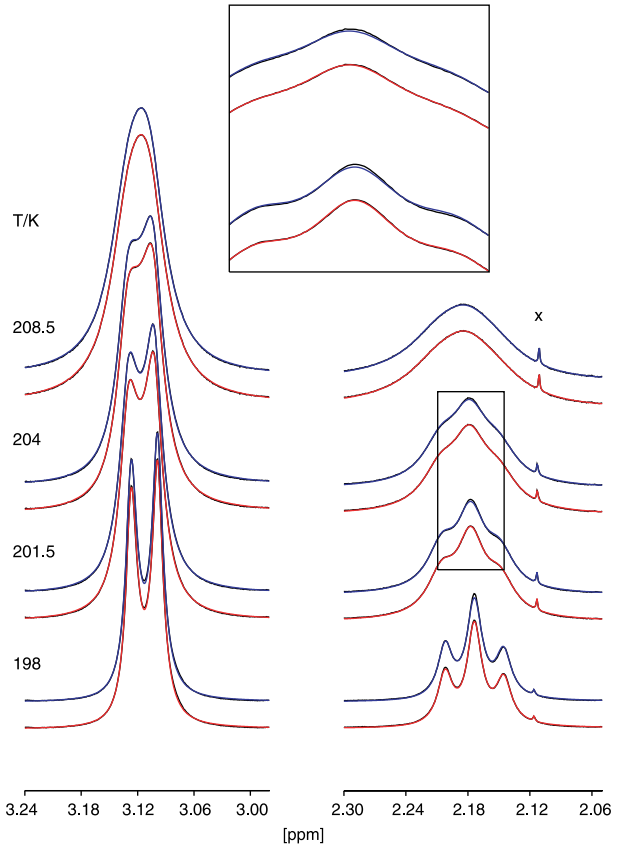

Fig. 2. The standard spectra of the methyl protons in TCDMT in the slow exchange limit superimposed with the "best fit" theoretical spectra. For each temperature, the top and bottom plots depict the AB and DQR fits, respectively. The impurity signals included in the fits, with assumed Lorentzian lineshape, are marked with x.

different from 1 as they oscillate in the range 1.08–1.13. Actually, the upper limit should be lowered to 1.09, since the only value exceeding 1.09, that of 1.132, was obtained at 198 K where the combined relaxation and field-inhomogeneity broadenings are still comparable to the exchange broadenings; the fits may therefore suffer some residual bias, as pointed out in the foregoing. Above 200 K, the bias is negligible. Attempts at an extraction of the values of c from the substantially broadened spectra above 220 K gave inconsistent results. The spectra above 220 K were analyzed under assumption that c is temperature-independent; the value of c was set equal to 1.085, the arithmetic average of the values obtained in the range 201–210 K. Similarly, above 209 K the average values of $|J| = 12.57$ Hz and, above 220 K, of $\delta_A - \delta_B = 416$ Hz (0.832 ppm) were assumed and kept fixed in the fits. The latter assumptions will be commented upon further later on. Above 220 K, the values of w were not adjusted; they were assumed equal to the average half-widths-at-half-heights of the aromatic proton signals.

The deficiencies of the AB fits, shown in Fig. 2, even when considered in the context of the evident perfection of the corresponding DQR fits, are too small to allow for a unequivocal discrimination between the two models. For this reason, we had to resort to the use of the CP-echo spectra. The fits to the echo spectra were performed with optimization of the pulse strength. A comparison of the AB and DQR fits to the sets of CP echo spectra measured at 201.5 and 204 K is shown in Fig. 3 for the signals of proton B. The deficiencies of the AB fits that are almost invisible for the standard spectra are now substantially amplified. On the other hand, a perfect reproduction of the experimental lineshapes could be achieved within the DQR model, where only one more adjustable parameter was added. For the signals of protons A_2 (not shown), both the fits seem equally perfect at a first sight, although some slight inferiority of the AB fits is still discernible for the spectra with longer echo times. The values of the relevant parameters, obtained in the DQR fits to the standard and echo spectra, are given in Table 1. In general, the differences between the results of fits to the standard and

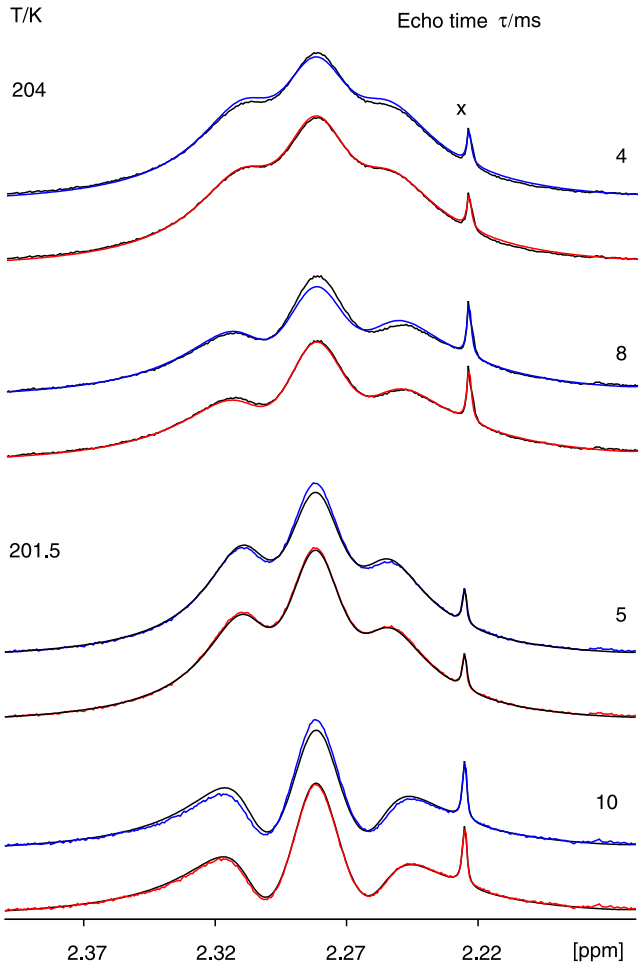

Fig. 3. The CP-echo spectra of the methyl proton B in TCDMT in the slow exchange limit superimposed with the "best fit" theoretical spectra. For each echo time, the top and bottom plots depict the AB and DQR fits, respectively.

Table 1
Results of iterative lineshape analysis of the standard and CP-echo spectra of 1,2,3,4-tetrachloro-9,10-dimethyltriptycene TCDMT[a]

T (K)	τ (ms)[b]	w (Hz)[c]	J (Hz)[c]	k_K (s^{-1})	$c = k_t/k_K^c$
198	0	1.56(1)	12.593(5)	20.4(1)	1.132(6)
198	5,10	1.51(1)	12.567(3)	25.3(1)	1.156(3)
201.5	0	1.53(1)	12.55(1)	52.4(2)	1.077(3)
201.5	5,10	1.48(1)	12.501(4)	51.9(1)	1.098(2)
204	0	1.51(1)	12.55(1)	70.0(3)	1.078(4)
204	4,8	1.49(1)	12.60(1)	69.3(2)	1.096(2)
208.5	0	1.37(2)	12.62(3)	128.2(6)	1.090(7)
208.5	3,6	0.97(2)	12.55(2)	129.1(3)	1.078(3)
210	0	1.48(2)	12.57	156(1)	1.077(5)
220.5	0	0.75	12.57	537(1)	1.085
231	0	0.70	12.57	1779(2)	1.085
242	0	0.60	12.57	4736(3)	1.085
251.5	0	0.60	12.57	10290(10)	1.085
259	0	0.55	12.57	19210(20)	1.085
265.5	0	0.50	12.57	30780(30)	1.085

[a] The standard errors, quoted in parentheses, were calculated with neglect of the possible statistical correlations between the fitted parameters.
[b] Echo times; $\tau = 0$ means standard spectrum.
[c] Numbers without standard errors are assumed values (see text).

CP-echo spectra are commensurate with the corresponding standard errors. (The standard errors quoted in Table 1 are calculated with a neglect of the off-diagonal elements of the Hessian matrix; as such, they are generally underestimated since the possible statistical correlations between the fitted parameters are ignored. A more elaborate error analysis is out of scope of the present paper.)

The foregoing evidence of the nonclassical character of the methyl group dynamics in TCDMT will be strengthened when it is presented against the background of our previous findings for other methyltriptycene derivatives. In Fig. 4, previously unpublished details of the fits to the spectra of TBMT are shown. For the latter compound, and also for TCMT, the deficiencies of the AB model are already visible for the standard spectra [8,9]. For TBMT and TCMT, the average values of c in the ranges 187–197 K and 179–187 K, respectively, are 1.18 and 1.19, respectively. For the investigated sample of TBMT, the spectral regions of interest happened to be free from intense impurity signals. This allowed us to exploit series of echo spectra covering a broader range of echo times. Just as in the fits for TCDMT, the realistic model of the radiofrequency pulses was used and the parameter ω_1 was adjusted. Thus, for the unquestionable inadequacy of the AB fit one can hardly blame imperfections of the experimental pulses. The problem of pulse modeling will be discussed in detail later on. Actually, the evident perfection of the DQR fits to the series shown in Fig. 4 once helped us to dispel ultimately our fears that the effects involved might have resulted from nonvanishing temperature gradients within the sample. We simulated possible effects of such gradients by producing variously weighted sums of the theoretical echo spectra calculated from the AB equation. The calculations were done for a number of values

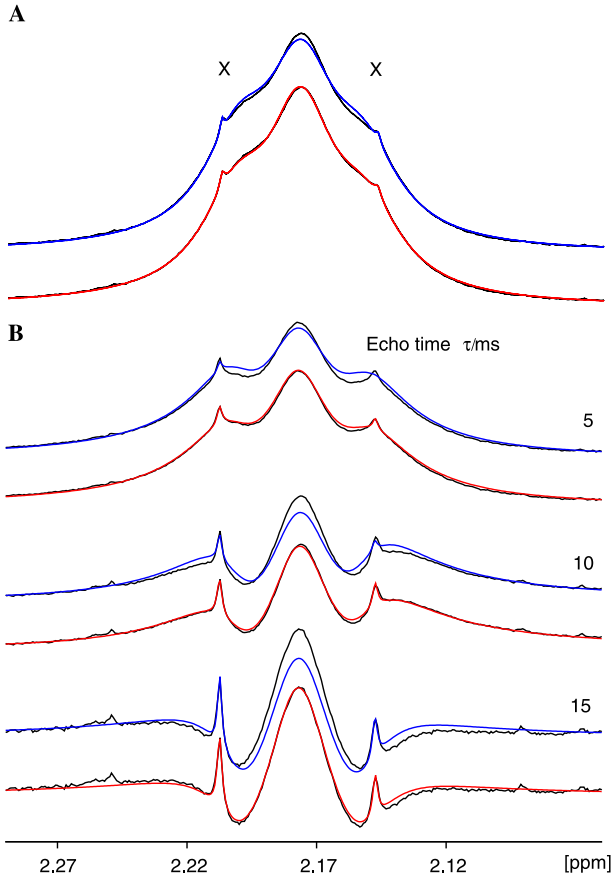

Fig. 4. (A) The standard spectra of the methyl protons in TBMT at 187 K superimposed with the "best fit" theoretical spectra obtained in the AB (top) and DQR (bottom) fits, respectively. (B) The corresponding CP-echo spectra superimposed with the "best fit" theoretical spectra. For each echo time, the top and bottom plots depict the AB and DQR fits, respectively.

of k covering some reasonable interval. Such artificial echo spectra were further subject to the DQR fits. The achieved reproducibility of the lineshapes involved was far from perfect. It seems that the actual deformations of the experimental spectra due to temperature gradients are minor. It seems that the resulting bias involves mainly the values of w which appear to be somewhat overestimated.

We could also exclude the eventuality that some residual ordering of the dissolved molecules, enforced by the external magnetic field, may be at stake: attempts at fitting the possible residual dipolar couplings as extra parameters in the AB model did not lead to a satisfactory improvement of the fits.

Now, the conclusion that the general nature of the stochastic dynamics must be the same for TCDMT and TBMT is confirmed by the evident similarity of the lineshape effects shown in Figs. 3 and 4. Some quantitative differences are discussed below. In Fig. 5, the values of J obtained in the fits for TBMT, TCMT, and TCDMT are plotted against temperature. A substantial dependence of J on temperature, observed for the two former compounds, was tentatively explained [9] in terms of the coherent tunneling [15–17]. A theoretical model of dependence of the coherent tunneling on temperature far above the cryogenic range has not been proposed yet. With such a model still lacking, for TBMT and TCMT we could not extrapolate the values of J to the temperatures where this parameter is no longer extractable from the broadened spectra. Unbiased fits were obtainable in relatively narrow temperature ranges of about 10 K only. For the compound investigated presently, the values of J do not show a clear dependence on temperature. It seemed thus reasonable to assume that in TCDMT the magnitude of J is controlled entirely by the usual electron-mediated mechanism so that dependence of J on temperature should be negligible. Hence, we could analyze the spectra from a wide temperature range, under an additional assumption that $\delta_A - \delta_B$ is also temperature-independent. The latter is suggested by the behavior of $\delta_A - \delta_B$ observed in the range 195–210 K. The assumption of c independent of temperature is arbitrary since no data about the behavior of c over wide temperature ranges are available for liquid-phase temperatures. The values of k_K determined under the above assumptions (see Table 1) present a fair linear alignment on the Arrhenius plot shown in Fig. 6. The activation energy and decimal log of the preexponential factor are 44.8(4) kJ/mol and 13.4(1), respectively. For a comparison, the Arrhenius activation energies once found for TCMT, TBMT, and 1,2,3,4,5,6,7,8-octachloro-9-methyltriptycene OCMT using the AB model are 39, 43, and 59 kJ/mol, respectively [10]. The values of c (1.19, 1.18, 1.09, and 1.01 for TCMT, TDMT, TCDMT, and OCMT, respectively) do not correlate strictly with the activation energies, although some qualitative relationship does occur. Generally, the quantum character of the stochastic dynamics should be more apparent for methyl groups with lower hindering potential. A closer identification of the structural factors that control the magnitude of c is one of our current research tasks.

The average value of $|J|$ in TCDMT, 12.57 Hz, coincides with the limiting, low-temperature value of this parameter in TCMT (see Fig. 5). For electron-mediated spin couplings such a coincidence could be expected since the immediate surroundings of the methyl groups are virtually identical in both the compounds. This provides an independent corroboration to our previous assessment that in TCMT the residual coherent tunneling must

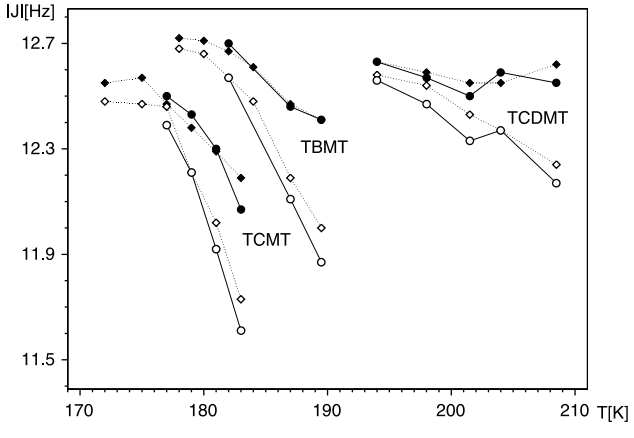

Fig. 5. Temperature dependences of the values of J obtained in the DQR (full symbols) and AB fits (open symbols) for TCMT, TBMT, and TCDMT. The values obtained from standard and CP-echo spectra are represented by diamonds and circles, respectively.

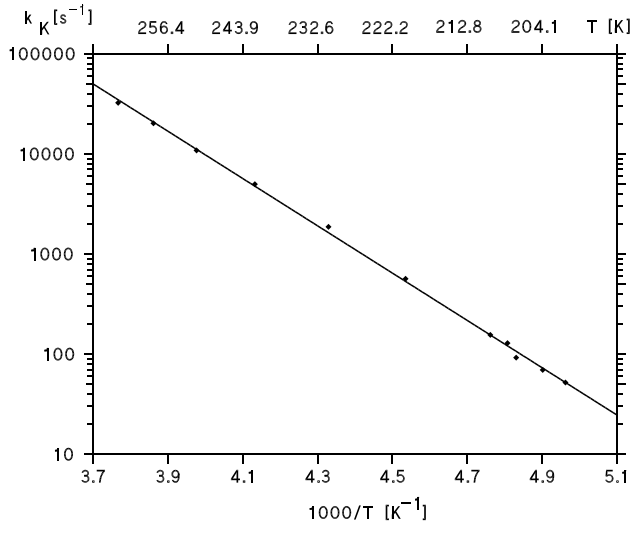

Fig. 6. The Arrhenius plot for rate constant k_K in TCDMT. Above 210 K, the data were obtained under assumption of $c = 1.085$. The activation energy and decimal log of the preexponential factor are 44.8(4) kJ/mol and 13.4(1), respectively, where the standard errors do not reflect inaccuracies in the temperature measurements.

vanish completely in the low temperature limit [9]. (From the fact that the dominating, magnetic component of $|J|$ is negative we could previously deduce the sign of the tunneling contribution in TCMT and TBMT to be positive; as is stated in [9], the latter cannot come from the splitting of the ground torsional state alone and the higher torsional states must be engaged.)

One more effect is apparent from the data in Fig. 5, which can serve as a valuable hint in future studies on the methyl rotation in liquid-phase NMR. When the spectra are interpreted in terms of the AB model, the adjusted values of $|J|$ show much stronger decrease with increasing temperature than those obtained from the DQR fits. For TCMT and TBMT, this artificial effect was already commented upon [9]. Now the same effect can be seen for TCDMT, the compound for which the unbiased estimates of J do not show any remarkable dependence on temperature. It seems that such a underestimation of the values of $|J|$ in the fitting process is a partial remedy to the inadequacy of the AB model, whose efficiency increases along with the progressing obliteration of the fine structure due to the J-couplings. Actually, when in the AB fits the value of $|J|$ is put equal to the average from the DQR fits (12.57 Hz) and is not optimized, the fit deficiencies are readily visible already for the standard spectra. It is noteworthy that for OCMT, for which the values of c are quite close to 1, such artificial temperature trend was not observed for the estimates of J obtained in AB fits. Therefore, a detection of such a trend in the results of AB fits may indicate that the underlying stochastic dynamics are nonclassical even when there are no clear discrepancies between the theoretical and experimental lineshapes.

Finally, we discuss the problem of pulse modeling in computer-aided interpretation of CP-echo spectra. In Fig. 7, the DQR fit to the set of three echo spectra, shown in Fig. 4, is compared with the similar fit performed under assumption of ideal radiofrequency pulses. The accuracy of the latter fit is evidently worse than of the former, which can be seen particularly clearly for the 15 ms-echo spectrum.

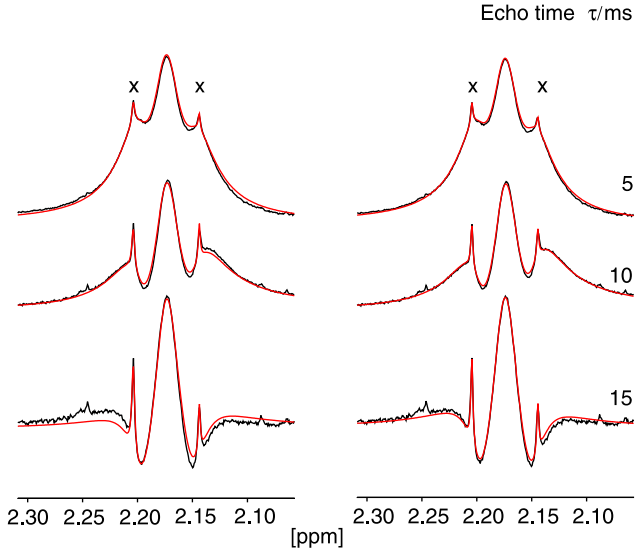

Fig. 7. A comparison of the DQR fits to the CP-echo spectra of TBMT at 187 K, obtained with assumed ideal pulses (left panel) and with optimized pulse strength (right panel).

In the experiment, the pulses were applied at 2.788 ppm. The lengths of the π- and $\pi/2$-pulses were set to 1/2 and 1/4, respectively, of the length of the 2π pulse, 33.6 μs, calibrated for the methyl proton doublet centered at 3.066 ppm (not shown). For perfectly rectangular pulses, the nominal strength of the RF field, $\omega_1/2\pi$, would be 29.76 kHz. In the DQR fit shown in Fig. 4 and in the right panel in Fig. 7, the optimized value of $\omega_1/2\pi$ is 27.47(1) kHz; in the AB fit (Fig. 4), the corresponding value is 27.20(2) kHz. In general, when ω_1 is included in the optimized set, there are two solutions of the least-squares problem for CP-echo spectra of the triptycene derivatives. It is dependent on the starting value of ω_1, which of the two solutions will be obtained at convergence. When the starting value of the latter is smaller (greater) than the nominal value, the final value will also be smaller (greater) than the nominal value. The adjusted values of ω_1 are symmetrically disposed around the nominal value; the corresponding minima on the sum-of-squares surface can have either the same or somewhat different depths. In any case, differences between the corresponding optimum values of the "global" parameters k_K, c, J, w, δ_A, and δ_B are commensurate with the standard errors involved. More pronounced differences occur for the "local" parameters which measure deviations from perfect phasing for the individual echo spectra in the fitted set. To avoid any ambiguities, as the correct values of the global parameters we always take the optimum values corresponding to the smaller of the two RMS errors. It must be stressed that we have never been faced with the situation where the RMS errors involved are (nearly) equal while the corresponding values of the parameters of interest are substantially different. A typical instance of such a double minimum on the sum-of-squares surface is illustrated in Table 2, where the pertinent fit results for the CP echo spectra of TBMT at 187 K are collected. The fit variants delivering under- and over-estimated values of ω_1 are numbered I and II, respectively; III denotes the fits with assumed ideal π- and $\pi/2$ pulses. From the data in Table 2 it is seen that for the DQR fits, the RMS errors in variants I and II are nearly identical. The values of the parameters of interest, obtained in these fits, are practically the same; in comparison with the standard errors involved, the greatest is the difference between the values of c. (The standard errors are probably underestimated, see the parenthetical comment above.) However, it is still small with respect to the typical scatter of the values of c obtained from the standard and CP-echo spectra. On the other hand, the

Table 2
Results of fits to the set of three CP-echo spectra ($\tau = 5$, 10, and 15 ms) of 1,2,3,4-tetrabromo-9-methyltriptycene TBMT at 187 K with optimization of RF pulse strength (variants I and II) and with assumed ideal pulses (variant III)

Fit variant	$\omega_1/2\pi$ (kHz)	w (Hz)	J (Hz)	k_K (s^{-1})	$c = k_t/k_K$	RMS error[a]
DQR I	27.49(1)	1.77(1)	12.447(4)	55.0(1)	1.169(1)	.335
DQR II	32.16(1)	1.78(1)	12.449(4)	54.5(1)	1.179(1)	.337
DQR III	—	1.32(1)	12.558(6)	59.3(2)	1.195(2)	.529
AB I	27.20(2)	2.44(2)	12.096(6)	54.9(2)	1	.617
AB II	32.42(2)	2.46(2)	12.081(6)	54.7(2)	1	.644
AB III	—	1.98(2)	12.15(1)	61.9(4)	1	.815

[a] As a percentage of max. amplitude of the experimental spectrum.

values of k_K, J, and w obtained in variant III are significantly different from their counterparts in variants I and II. Note a dramatic increase of the RMS error in variant III as compared to I and II; this is visualized in Fig. 7. It must be added that for sets of CP-echo spectra covering a narrower range of echo times the differences between the particular fit variants are in general smaller than in the case depicted in Fig. 7. For the CP-echo spectra of TCDMT (Fig. 3), there is virtually no differences between the values of k_K, c, J, δ_A, and δ_B obtained in variants I and II, although the RMS errors in variant I are consistently lower by about 2–3% than in variant II.

In summary, despite of some difficulties involving the possible doubling of the least-squares solutions, use of realistic models of the radiofrequency pulses can be recommended when series of CP-echo spectra are to be analyzed. The discriminative potential of such an approach with respect to alternative models of molecular rate processes was shown on the example of the methyl group dynamics in TCDMT. With arguments derived solely from the standard spectra, the quantum character of that process could not be demonstrated convincingly. By and large, the argument revealing the true origin of the effect discussed in this paper is ultimately based on the fact that the evidently flawed AB fits to the echo spectra can be confronted with the perfect DQR fits. In the approach with assumed ideal pulses, where neither of the two descriptions is perfect, the situation would be less clear and there might still be a room for speculations about alternative explanations of the effect.

Acknowledgment

This work was supported by the State Committee for Scientific Research (KBN) under Grant 7T09A06520.

References

[1] K.G. Orrel, Ann. Rep. NMR Spectrosc. 37 (1999) 1.
[2] S. Szymański, J. Chem. Phys. 111 (1999) 288.
[3] S. Alexander, J. Chem. Phys. 37 (1962) 967.
[4] D.A. Kleier, G. Binsch, J. Magn. Reson. 3 (1970) 146.
[5] H.Y. Carr, E.M. Purcell, Phys. Rev. 94 (1954) 630.
[6] R. Freeman, Spin Choreography. Basic Steps in High Resolution NMR, chapter 4, Oxford University Press, Oxford, 1998.
[7] S. Szymański, Z. Olejniczak, A. Detken, U. Haeberlen, J. Magn. Reson. 148 (2001) 277.
[8] P. Bernatowicz, S. Szymański, Phys. Rev. Lett. 89 (2002) 023004.
[9] I. Czerski, P. Bernatowicz, J. Jaźwiński, S. Szymański, J. Chem. Phys. 118 (2003) 7157.
[10] M. Nakamura, M. Oki, H. Nakanishi, O. Yamamoto, Bull. Chem. Soc. Jpn. 47 (1974) 2415.
[11] A.L. Van Geet, Anal. Chem. 40 (1968) 2227.
[12] C.S. Johnson, J. Chem. Phys. 41 (1964) 3277.
[13] S. Szymański, J. Magn. Reson. A 115 (1995) 254.
[14] P. Bernatowicz, S. Szymański, J. Magn. Reson. 164 (2003) 60.
[15] F. Apaydin, S. Clough, J. Phys. C. Ser. 2 1 (1968) 932.
[16] C. Mottley, T.B. Cobb, C.S. Johnson, J. Chem. Phys. 55 (1971) 5823.
[17] A.J. Horsewill, Prog. Nucl. Magn. Reson. Spectrosc. 35 (359) (1999).
[18] R.S. Dumond, S. Jain, A.D. Bain, J. Chem. Phys. 106 (1997) 5928.